

Iron(IV) Complexes with Tetraazaadamantane-based Ligands: Synthesis, Structure, Application in Dioxygen Activation and Labeling of Biomolecules

Ivan S. Golovanov,^a Anton V. Leonov,^{a,b} Vladislav K. Lesnikov,^a Evgeny V. Pospelov,^{a,b} Kirill V. Frolov,^c Alexander A. Korlyukov,^d Yulia V. Nelyubina,^d Valentin V. Novikov,^d Alexey Yu. Sukhorukov^{a,e,f,*}

^a N. D. Zelinsky Institute of Organic Chemistry, Russian Academy of Sciences, Leninsky prospect, 47, Moscow, Russia, 119991

^b M. V. Lomonosov Moscow State University, Leninskiye Gory, 1, Moscow, Russia, 119991

^c Shubnikov Institute of Crystallography of FSRC "Crystallography and Photonics", Russian Academy of Sciences, Leninsky prospect, 59, Moscow, Russia, 119991

^d A. N. Nesmeyanov Institute of Organoelement Compounds, Russian Academy of Sciences, Vavilov str. 28, Moscow, Russia, 119991

^e Plekhanov Russian University of Economics, Stremyanny per. 36, Moscow, Russia, 117997

^f D. Mendeleev University of Chemical Technology of Russia, Miusskaya sq. 9, Moscow, Russia 125047

Corresponding author*: Alexey Yu. Sukhorukov; orcid.org/0000-0003-4413-9453; e-mail: sukhorukov@ioc.ac.ru

Abstract

4,6,10-Trihydroxy-1,4,6,10-tetraazaadamantane (TAAD) has been shown to form a stable Fe(IV) complex having a adamantane cage structure, in which the metal center is coordinated by three oxygen atoms of the deprotonated ligand. The complex was characterized by X-ray, HRMS, NMR, FT-IR, Mössbauer spectroscopy and DFT calculations, which supported d^4 configuration of iron. The Fe(IV)-TAAD complex showed excellent performance in dioxygen activation under mild conditions serving as a mimetic of the thiol oxidase enzyme. The nucleophilicity of the bridge-head nitrogen atom in TAAD provides a straightforward way for conjugation of Fe(IV)-TAAD complexes to various functional molecules. Using this approach, steroidal and peptide molecules having an iron(IV) label have been prepared for the first time. Also, the Fe(IV)-TAAD complex was covalently bounded to a polystyrene matrix and the resulting material was shown to serve as a heterogeneous catalyst for aerobic oxidation of thiols to disulfides.

Introduction

High-valent iron species play a primary role in dioxygen activation catalytic cycles in biological processes.¹⁻⁴ The efficiency of these natural enzymes prompted scientists to develop bio-inspired artificial catalysts for efficient oxidation of organic substrates preferably with atmospheric oxygen as oxidant.⁵⁻¹⁰ Although this goal remains elusive at the moment, much research has been done in the field of high-valent, and in particular, Fe(IV) complexes.^{11, 12} In recent years, numerous high-valent iron complexes including heme- and non-heme Fe(IV) and Fe(IV)-oxo/nitride complexes, which mimic the structure and activity of natural oxidases have been generated and characterized.¹³⁻¹⁹ However, these species are generally unstable under ambient conditions in aqueous solution, thus complicating their study and application. The design of aqueous stable Fe(IV) complexes is challenging as structural factors, which stabilize

highly oxidized iron center are not completely understood. Few impressive examples of Fe(IV) complexes that exhibit infinite stability in water have been reported (Figure 1). One example is the hexahydrazide clathrochelate iron(IV) complex **I** prepared by Fritsky et al.^{20, 21} Another example is an iron(IV) complex with formaldoxime cyclotrimer (TFOH₃) **II**, which was recently prepared by our group.²² Surprisingly, both complexes **I** and **II** are formed by oxidation with air and their reduction to Fe(III) requires strong reducing agents. This demonstrates an extremely high stabilization of the oxidized iron center by both ligands. The reasons for such stabilization are not completely understood, yet the presence of a two-heteroatom bond (N–N or N–O) is believed to be essential.²² Thus, in order to gain an understanding of structural factors governing this stabilization further research in the field of Fe(IV) complexes with other polyhydrazine and polyhydroxylamine ligands has to be undertaken. Here, we report the preparation of a new stable Fe(IV) complex with tris-hydroxylamine ligand TAAD, its structural and electronic characterization and studies of its catalytic activity in aerobic oxidation of thiols. Furthermore, conjugation of this Fe(IV)-TAAD complex to biomolecules and solid support was demonstrated in this work.

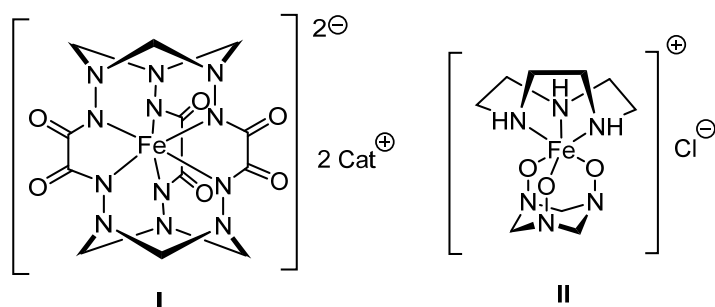


Figure 1. Examples of aqueously stable Fe(IV) complexes

Results and discussion

TAAD (4,6,10-trihydroxy-1,4,6,10-tetraazaadamantane, Figure 2) is a polydentate bench-stable ligand, which was synthesized in our laboratory some time ago.²³ Although the coordination chemistry of TAAD is poorly explored, it has been shown by us²⁴ and others^{25, 26} that TAAD can exhibit O^3 -coordination mode in boron and manganese complexes upon deprotonation in a similar fashion to TFOH₃. In contrast to TFOH₃ and related *N*-hydroxy amins, TAAD exhibits exceptional chemical stability attributed to the presence of an adamantane cage.²⁴ Moreover, TAAD can serve as a modifiable platform ligand, which can be easily functionalized with electrophilic agents at the bridgehead nitrogen atom N1 under very mild conditions. This can be used for covalent immobilization of the ligand on solid matrixes or for the construction of modular conjugates of TAAD with biomolecules.^{27, 28} Given the aforementioned importance of Fe(IV) complexes, we studied the complexation of iron with TAAD under an aerobic atmosphere.

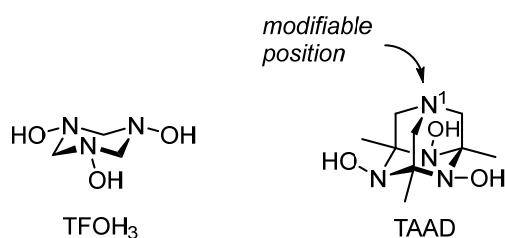
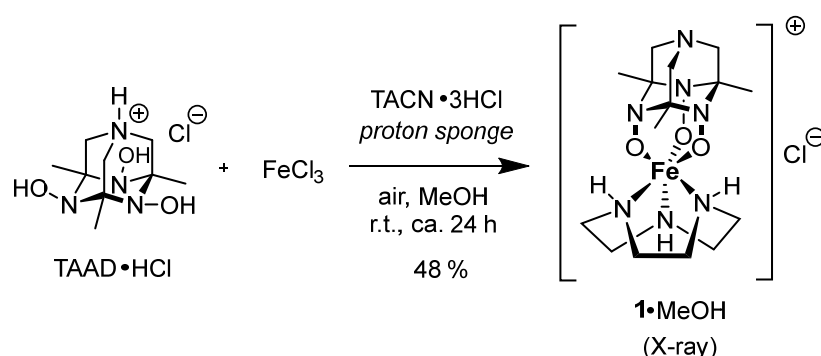


Figure 2. Structures of tris-hydroxylamine ligands TFOH₃ and TAAD

Synthesis of Iron(IV)-TAAD Complex

Initially, TAAD hydrochloride was reacted with FeCl₃ in methanol in the presence of an organic base (1,8-bis(dimethylamino)naphthalene, “proton sponge”) under air. Immediate darkening of

the reaction mixture was observed, however, attempts to isolate any complexes by crystallization from the reaction mixture failed. Performing the reaction in the presence of a supporting macrocyclic ligand (TACN, taken as a trihydrochloride salt) was more advantageous and provided a deep brown crystalline material with strong adsorption at 496 and 577 nm. Elemental analysis and high-resolution mass-spectra revealed the 1 : 1 : 1 (Fe/TAAD/TACN) composition of the complex **1** (Scheme 1).



Scheme 1. Synthesis of iron(IV) complex with TAAD ligand. TACN – 1,4,7-triazacyclononane; *proton sponge* – 1,8-bis(dimethylamino)naphthalene.

Complex **1** is well-soluble in methanol, water, and DMF and poorly soluble in aprotic low polar organic solvents. The complex is relatively stable upon storage on air at ambient conditions. Slow decomposition was observed upon storage both in solution (changes in UV-Vis spectra are feasible after ca. 1 week) and in solid-state (ca. 20 % after 100 days according to Mössbauer spectra and X-ray powder diffraction analysis).

X-ray analysis and IR-spectroscopy

X-ray analysis of complex **1** showed an unprecedented diamantane-like structure, in which octahedral iron atom occupies apical position being coordinated by three oxygen atoms of TAAD (Figure 3). The other three vacancies of metal are occupied by three nitrogen atoms of TACN. The coordination geometry around the metal ion is close to an ideal octahedron, as follows from continuous symmetry measures ($S(\text{OC})$ and $S(\text{TPR})$ evaluated from the X-ray diffraction data are 0.309 and 14.007). In the outer sphere of the complex, chloride anion and methanol molecule were present. Hydroxyl groups of TAAD were deprotonated suggesting the +4 formal oxidation state of the iron center.

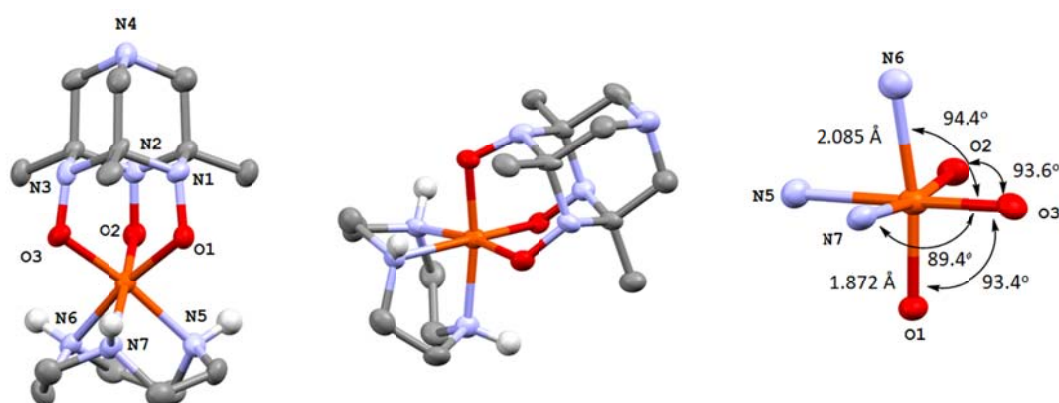


Figure 3. Principal structural motif and details of geometry around the metal center in complex **1**. CH-hydrogen atoms are omitted for clarity.

The Fe–O bonds are rather short (1.87 Å) and close to previously reported iron complexes with deprotonated hydroxylamines.^{29–31} The N–O bonds (1.38 – 1.40 Å) are shortened compared to the initial TAAD ligand (1.44 – 1.46 Å). The presence of a strong band appearing at 965 cm^{–1} in the IR-spectra is also indicative of an N–O bond in transition metal complexes of deprotonated

hydroxylamines and in iron(IV) complex with formaldoxime cyclotrimer (TFOH₃) II.²² Overall, the observed structural metrics and IR-spectroscopy data are more consistent with Fe...(⁻O–N) motif rather than with iron-nitroxide bonding Fe...([•]O–N).^{22,32}

Electronic structure of iron(IV)-TAAD complex

The electronic structure of complex **1** was studied by means of Mössbauer spectroscopy, paramagnetic NMR spectroscopy (Evans method) and DFT calculations. The ⁵⁷Fe Mössbauer spectra recorded at 295 K features a quadrupole doublet with an isomer shift $\delta = 0.275$ mm/s and a quadrupole splitting $|\Delta E_Q| = 3.209$ mm/s (Figure 4, Table 1). The Mössbauer spectra taken between 10 and 295 K indicate that the hyperfine parameters change almost linearly as the temperature increases (Table 1). The observed hyperfine parameters of Mössbauer spectra are consistent with the values expected for quasi-octahedral Fe(IV) complexes with $S = 1$.^{14, 20, 22} Large quadrupole splitting values point to a relatively high value of an electric field gradient presumably arising from stretching along the axis of the gradient.

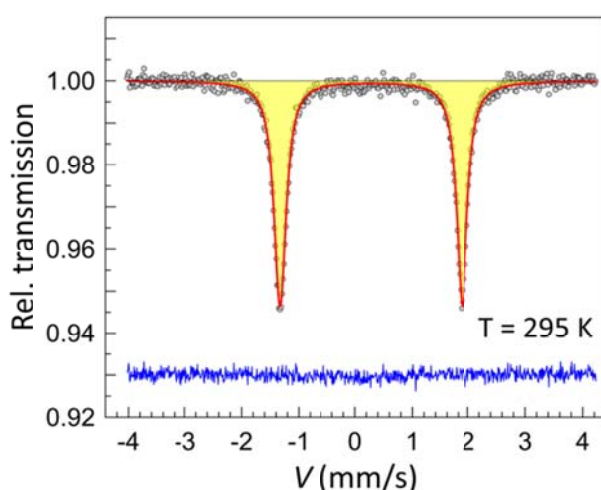


Figure 4. Mössbauer spectrum of iron(IV)-TAAD complex **1**

Table 1. Experimental and calculated (DFT) Mössbauer parameters of iron(IV)-TAAD complex **1**

Approach	<i>S</i>	T, K	δ (mm/s)	ΔE_Q (mm/s)	Γ (mm/s)
experiment	-	295	0.28	3.21	0.26
experiment	-	180	0.34	3.20	0.27
experiment	-	80	0.35	3.19	0.27
experiment	-	10	0.36	3.18	0.26
calculation ^a	1	-	0.24	-2.21	-
calculation ^a	0		0.21	-1.48	-
calculation ^a	2	-	0.47	-1.00	-

T – temperature, δ – isomer shift, ΔE_Q – quadrupole splitting, Γ – full width at half-maximum of the signal. ^a RHO was calculated with B3LYP DFT functional using CP(PPP) basis set on Fe and def2-TZVP basis set on other atoms. Electric field gradient was calculated using TPSS DFT functional with DKH-def2-QZVPP basis set on Fe and def2-TZVP basis set on other atoms was used. Relativistic effects were taken into account by requesting a Douglas-Kroll-Hess 2nd order scalar relativistic calculation. Calculations were performed for the DFT-optimized structure (DFT-D3 level of theory with BP86 functional and jorgeTZP basis set was used for geometry optimization and calculations of thermochemistry).

According to DFT calculations performed at the DFT-D3 level of theory with the BP86 functional, the structure of complex **1** having two unpaired electrons ($S = 1$) was predicted to be the most stable. Hypothetic low spin ($S = 0$) and high spin complexes ($S = 2$) were separated from $S = 1$ configuration by 9.1 and 14.4 kcal/mol, respectively. The geometry parameters of low spin and intermediate spin structures are in good agreement with X-ray data, while the

structure with $S = 2$ shows substantial deviation from the experiment. On the other hand, calculated Mössbauer parameters (δ and ΔE_Q) for complex with $S = 1$ are closer to experimental values compared to low spin ($S = 0$) and high spin structures ($S = 2$) (cf. data in Table 1). Thus, computation studies support the structure with two unpaired electrons. Mulliken population analysis of complex with $S = 1$ shows that the spin density is almost totally localized on the iron atom (1.83 of 2 electrons) as can be seen in Figure 5.

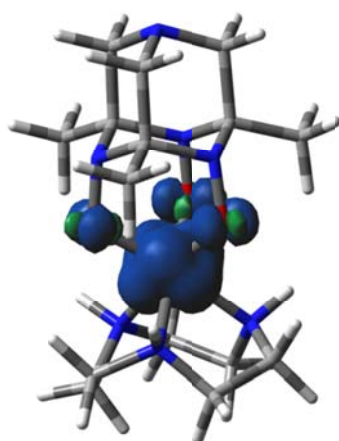


Figure 5. Calculated spin density in iron(IV)-TAAD complex **1**

The ground state electronic configuration predicted by DFT calculations was confirmed by paramagnetic NMR studies. The magnetic susceptibility χT of complex **1** measured by the Evans method was $1.58 \text{ cm}^3 \times \text{mol}^{-1} \times \text{K}$, which is close to the spin-only value for $S = 1$ ($\chi T = 1.00$). A relatively narrow character of the signals indicates that the spin density is mostly localized on the iron and not on the ligand.

Thus, the obtained experimental and computational data provide strong evidence for the assignment of the ground state electron configuration close to d^4 with $S = 1$ for the iron atom in complex **1**.

Electrochemical properties

The cyclic voltammogram (CV) of iron(IV)-TAAD complex **1** measured in dimethylformamide with tetrabutylammonium hexafluorophosphate solution as a supporting electrolyte is shown in Figure 6. CV revealed one irreversible oxidation wave (with E_0 equal to 0.4 V referenced to the Fc/Fc^+ couple) and one quasi-reversible reduction feature at $E_0 = -0.5$ V. The increase in the scan rate led to a quasi-reversible behavior in the case of the oxidation wave, while an additional wave in the reduction region remained irreversible even at scan rate $1 \text{ V} \times \text{s}^{-1}$.

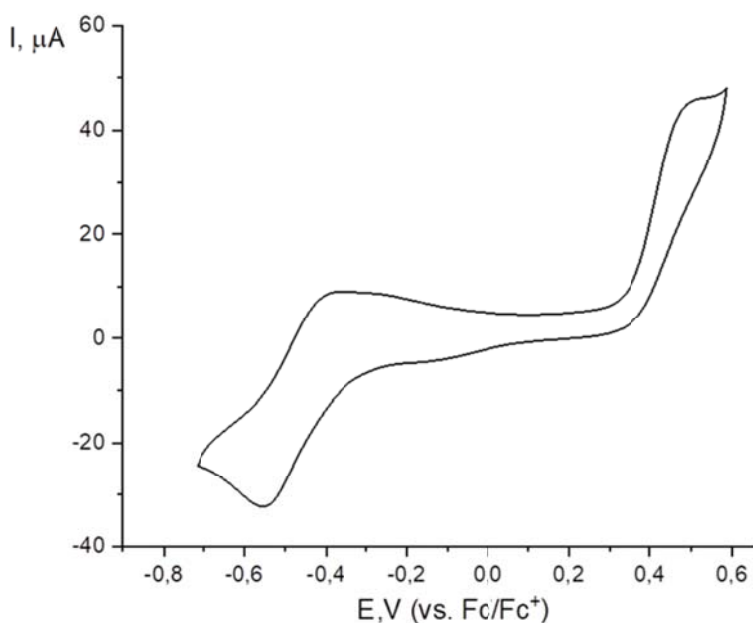


Figure 6. Electrochemical data for a 1 mM dimethylformamide solution of complex **1** with 0.1 M $(n\text{-C}_4\text{H}_9)_4\text{N}^+\text{PF}_6^-$ as a supporting electrolyte. Conditions: scan rate $100 \text{ mV} \times \text{s}^{-1}$, 298 K, platinum working and counter electrodes, Ag/AgCl reference electrode, the potentials are references to Fc/Fc^+ couple.

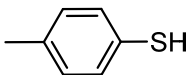
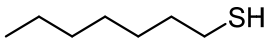
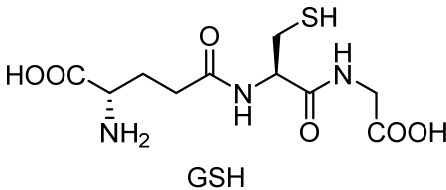
The negative reduction potential exhibited by complex **1** demonstrates the ability of the deprotonated TAAD ligand to stabilize the Fe(IV) oxidation state. However, the absolute value is smaller compared to previously reported hexahydrazide clathrochelate iron(IV) complex **I** and iron(IV) complex with formaldoxime cyclotrimer (TFOH₃) **II**, which have a similar octahedral environment (E_0 ca. -1.0 V).^{20, 22} Thus, iron(IV)-TAAD complex **1** is expected to be a stronger oxidant. This may also account for the observed slow degradation of complex **1** both in solution and in solid-state, plausibly via oxidation of the TAAD ligand.

Catalytic activity in aerobic oxidation

Oxidation of thiols to disulfides is an important reaction both in biological processes³³ (e.g. glutathione/glutathione disulfide redox couple³⁴) and in the industrial preparation of some pharmaceuticals and agrochemicals.^{35, 36} In nature, the formation of disulfide linkage from two thiol molecules is accomplished with air under catalysis with thiol oxidase enzyme, while in chemical synthesis stoichiometric oxidants are typically used for this transformation. From the environmental viewpoint, the development of efficient catalytic methods that mimic thiol oxidase activity and utilize air as the only oxidant is highly desirable.^{37, 38} Few catalysts based on iron compounds have been reported recently, yet their performance is limited by high loadings.^{37, 39} Since iron(IV)-TAAD complex **1** is generated by aerobic oxidation, we speculated that species resulting from its reduction can be readily re-oxidized with air. Thus, a catalytic cycle can be designed. With this in mind, the catalytic activity of iron-TAAD complex **1** in aerobic oxidation of thiols to disulfides was investigated (Table 2). With only 1 mol% of complex **1**, full conversion of *p*-thiocresol was achieved within 24 h. Aliphatic thiols proved to be somewhat less reactive in this catalytic oxidation process and 5 mol% of complex **1** was needed

for a complete conversion of *n*-heptanethiol and glutathione (GSH) to the corresponding disulfides (Table 2).

Table 2. Aerobic oxidation of thiols catalyzed by iron-TAAD complex **1**

$\text{R-SH} \xrightarrow[\text{rt, 24 h}]{\text{complex } \mathbf{1} \text{ (mol \%)} \atop \text{air (balloon)}} \text{R-S-S-R}$		
Thiol	Conditions	Yield ^a (conversion)
	1 mol% cat. 1 , Et ₃ N (1 equiv.), MeOH	84 % (> 99 % ^b)
	5 mol% cat. 1 , Et ₃ N (1 equiv.), MeOH	72 % (> 99 % ^b)
	5 mol% cat. 1 , NaHCO ₃ (3 equiv.), H ₂ O	83 % (> 95 % ^c)

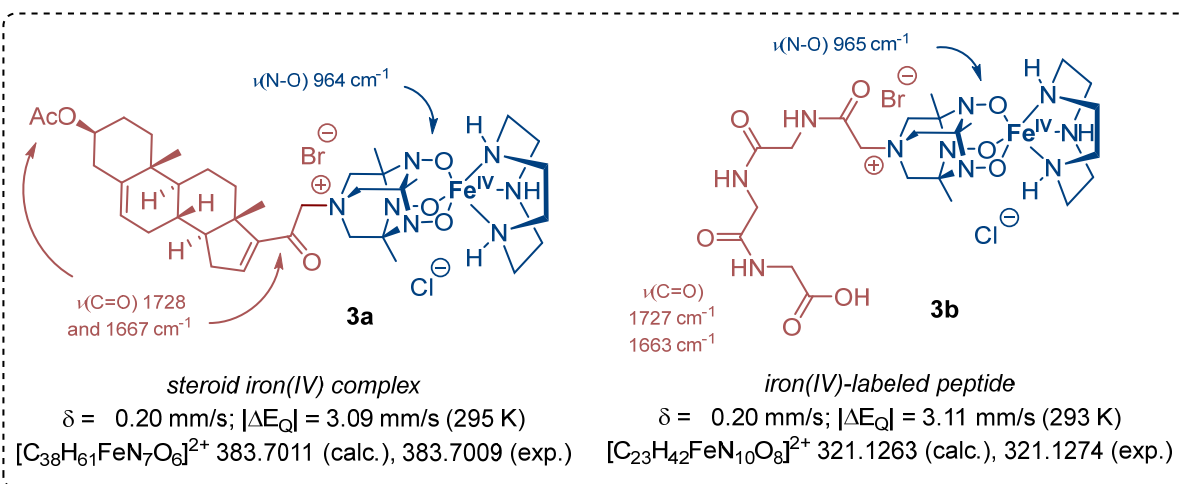
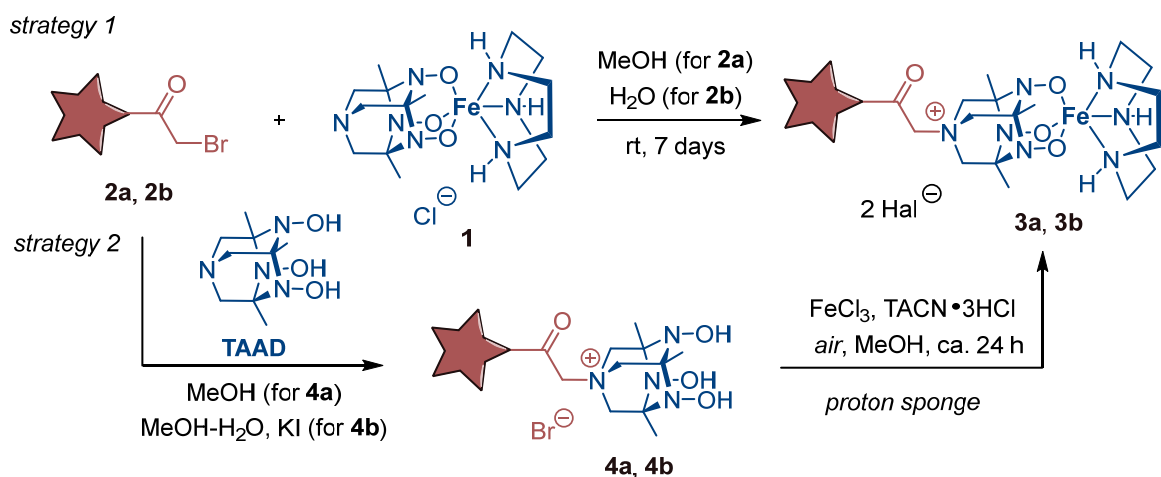
^a Yield of isolated material; ^b Determined by GC-MS; ^c Determined by ¹H NMR.

Overall, the catalytic activity of complex **1** is close to the most active iron-based catalysts reported in the literature to date.^{37, 39}

Conjugation of iron(IV)-TAAD complex with biomolecules and solid support

Due to a presence of a nucleophilic bridge-head nitrogen atom in the TAAD ligand, conjugation of complex **1** to various functional molecules can be performed in a straightforward manner. Two strategies can be sought to access modular structures containing iron(IV)-TAAD complex **1** as a functional unit (Scheme 2). In the first one, derivatization of complex **1** is done by its direct alkylation with a suitable electrophilic agent. In the second strategy, quaternization of TAAD with an electrophilic agent is initially performed,⁴⁰ and the resulting modified ligand is used to prepare a complex. Both strategies were tested to prepare conjugates, in which iron(IV)-TAAD complex **1** is bound to a biomolecule, such as a steroid and a short peptide. Steroid metal complexes have gathered attention as attractive vectors to deliver transition metal ions into specific cells (especially, tumor cells).⁴¹ In this context, high-valent metal species are of particular interest due to their cytotoxicity. On the other hand, metal-labeled peptides serve as models for metalloproteins as well as agents for diagnostic imaging and medical therapeutic treatment.⁴² To our knowledge, steroid and peptide iron(IV) complexes have not been described previously.

According to the first strategy, iron(IV)-TAAD complex **1** was reacted with androstane and triglycine (GlyGlyGly) derivatives **2a** and **2b** bearing a primary bromomethyl group (Scheme 2). Both reactions led to the formation of the desired conjugates **3a** and **3b** as evidenced by HRMS, FT-IR and Mössbauer spectroscopy. In comparison with Mössbauer parameters of the initial complex **1**, a characteristic shift of δ by 0.05 – 0.07 mm/s and a decrease of quadrupole splitting by ca. 0.1 mm/s was observed upon quaternization of the N1 nitrogen atom. However, Mössbauer spectra of conjugates **3** contained additional signals corresponding to unidentified iron species suggesting that partial decomposition of complex **1** could take place during the synthesis (plausibly, attributed to a prolonged reaction time).

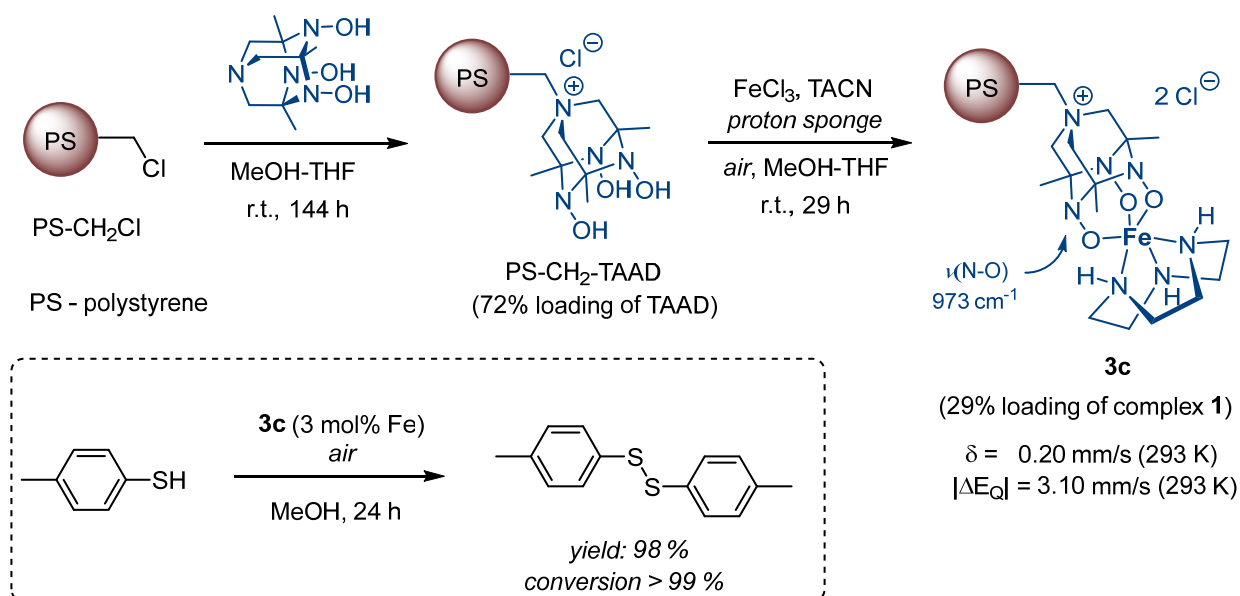


Scheme 2. Conjugation of Fe(IV)-TAAD complex **1** to biomolecules

The decomposition issue could be overcome, by implementing the second strategy. Initially, TAAD was conjugated to the corresponding androstane and triglycine derivatives **2a** and **2b** by a nucleophilic substitution reaction (Scheme 2). The resulting quaternary salts **4a** and **4b** containing a TAAD-based chelating motif were then reacted with FeCl₃, TACN and proton sponge under air to give the desired complexes **3a** and **3b**. Compared to strategy 1, the formation of **3a** and **3b** required less time (ca. 24 h) and the purity of these complexes was

much higher. Thus, strategy 2 was found to be more advantageous to perform the derivatization of iron(IV)-TAAD complex **1**.

High catalytic activity of complex **1** in aerobic oxidation of thiols (Table 2) prompted us to design a heterogeneous catalyst for this process. Thus, we sought of covalent immobilization of complex **1** on a solid support such as polystyrene (PS) using derivatization strategy 2. Hence, TAAD was reacted with Merrifield resin (PS-CH₂Cl) to give a polymer PS-CH₂-TAAD (Scheme 3).²⁷ Subsequent treatment of this resin with FeCl₃, TACN and proton sponge under air produced a brown-color polymeric material **3c** containing complex **1** covalently bounded to a polystyrene matrix. The presence of complex **1** residues in polymer **3c** was proven by characteristic features in Mössbauer spectra (δ = 0.20 mm/s, $|\Delta E_Q|$ = 3.10 mm/s at 293 K), as well as by IR-spectroscopy and elemental analysis.



Scheme 3. Synthesis of polymer-supported iron(IV)-TAAD complex **3c**. Conversion was determined by GC-MS.

Impressively, polymer **3c** exhibited pronounced catalytic activity in aerobic oxidation of *p*-thiocresol. Complete conversion to disulfide was achieved within 24 h with only 3 mol% of Fe.

Conclusion

In conclusion, we have shown that the TAAD ligand forms a stable Fe(IV) complex upon reaction with FeCl₃ and a supporting ligand (TACN). Unusually, the oxidation of Fe(III) to Fe(IV) in this reaction occurs with air as an oxidant. In the obtained complex, deprotonated TAAD ligand exhibits *O*³-coordination mode forming a symmetrical metallodiamantane structure. The structure of Fe(IV)-TAAD complex was studied by X-ray, HRMS, NMR, FT-IR, Mössbauer spectroscopy, X-ray powder diffraction analysis and DFT calculations, which supported d⁴ configuration of iron. The metallodiamantane scaffold in Fe(IV)-TAAD complex can serve as a modifiable platform, to which functional units can be attached by electrophilic addition at the bridgehead nitrogen atom. Using this approach, steroidal and peptide iron(IV) complexes have been prepared for the first time. Fe(IV)-TAAD complex exhibits catalytic activity in aerobic oxidation of thiols to disulfides serving as a mimetic of thiol oxidase enzyme. A heterogeneous catalyst for this process was developed by immobilization of Fe(IV)-TAAD complex on a polystyrene matrix.

Experimental section

General Methods and Instrumentation

All reactions were carried out in oven-dried (150°C) glassware. CH₂Cl₂ and Et₃N were distilled over CaH₂; THF was distilled over LiAlH₄; other solvents were distilled without drying agents. TAAD,²³ TAAD·HCl,⁴³ (3β)-21-Bromo-20-oxopregna-5,16-dien-3-yl acetate (**2a**),⁴⁴ quaternary salt **4a**,⁴⁰ 2-bromoacetyl

chloride⁴⁵ and polymer PS-CH₂-TAAD²⁷ were prepared according to previously described protocols. 1,4,7-Triazacyclononane trihydrochloride (TACN·3HCl), 1,8-bis(dimethylamino)naphthalene (proton sponge), glycylglycylglycine, *p*-thiocresol, *n*-heptanethiol, glutathione and all inorganic reagents were commercial grade and used as received.

NMR spectra were recorded at room temperature with residual solvent peaks as internal standards. Multiplicities are indicated by s (singlet), d (doublet), dd (doublet of doublets), t (triplet), m (multiplet), and br (broad). ¹H NMR spectra of complex **1** were recorded from CD₃OD solutions with a Bruker Avance 400 spectrometer. Data acquisition and processing were performed with Topspin 2.1 and Mestrenova 12.0.0 software, respectively. The magnetic susceptibility of the paramagnetic iron complex **1** in a CD₃OD solution was evaluated by the Evans method⁴⁶ at 305 K using a Wilmad NMR tube with a coaxial insert. The inner (reference) tube was filled with CD₃OD with approximately 1% of Me₄Si, the outer tube contained a CD₃OD solution of the paramagnetic complex **1** with a known concentration and the same amount of Me₄Si. The molar magnetic susceptibility was calculated from the difference between the chemical shift of Me₄Si in pure CD₃OD and its shift in the CD₃OD solution of the paramagnetic complex by the standard Evans method procedure.⁴⁷ The molar diamagnetic contribution to the paramagnetic susceptibility was estimated using Pascal's constants.⁴⁸

Melting points were determined on a Kofler heating stage and were not corrected. HRMS measurements were performed on a mass-spectrometer with electrospray ionization and a time-of-flight (TOF) detector. Peaks in FT-IR spectra data are reported in cm⁻¹ with the following relative intensities: s (strong), m (medium), w (weak), br (broad), sh (shoulder). UV-Vis spectra were recorded on a SF2000 spectrophotometer for the solutions of the investigated compounds. GC-MS was performed on a Chromatec 5000 with an Agilent DB-1MS column 122-0132.

Cyclic voltammetry (CV) experiments were performed for dimethylformamide solutions with 0.1 M tetrabutylammonium hexafluorophosphate as a supporting electrolyte using a Metrohm Autolab PGSTAT128N potentiostat with a conventional one-compartment three-electrode cell (5 mL of solution). Platinum disk electrode (MF-2013, BASi), which was used as a working electrode, was thoroughly

polished with 0.05 μm alumina slurry, sonicated for two minutes in deionized water and rinsed before every measurement. A platinum wire counter electrode and a standard $\text{Ag}/\text{AgCl}/\text{NaCl}_{(\text{aq})}$ reference electrode (RE-5B, BASi) were used. To account for a drift of the reference electrode, the ferrocene was added after the measurements as an internal standard, and all the potentials are reported relative to the Fc/Fc^+ redox couple. The solutions were thoroughly deaerated by passing argon through them before the CV experiments and above these solutions during the measurements.

^{57}Fe Mossbauer absorption spectra of powdered samples were recorded using a conventional constant-acceleration Mössbauer spectrometer MC-1104Em equipped with the closed-cycle helium cryostat RTI CryoFree-104.⁴⁹ Spectra were recorded without external magnetic field at atmospheric pressure and within temperature range from 10 K to 295 K in transmission geometry with a $^{57}\text{Co}(\text{Rh})$ source (MCo7.114). For a recording of Mossbauer absorption spectrum 50 mg of powdered sample was put into thin aluminum container (tablet) with approx. square 0.3 cm^2 . The plane of the tablet was placed perpendicular to the direction of γ -rays propagation. Isomer shifts are given relative to an α -Fe foil (30 μm MRA.2.6). Simulations of the experimental data were performed with the Univem MS program.

X-ray diffraction experiments were carried out at 120 K with a Bruker APEX2 DUO CCD diffractometer, using graphite monochromated Mo- $K\alpha$ radiation ($\lambda = 0.71073 \text{ \AA}$). CCDC 2110176 contains the supplementary crystallographic information for complex **1**. The powder X-ray diffraction patterns of the sample were measured in reflection mode. The measurements were performed with a Bruker D8 Advance diffractometer equipped with motorized slits and a LynxEye 1D position-sensitive detector. The measurement range was 4–60° in 2θ angle. All calculation was carried out with TOPAS 4.2 software.⁵⁰

DFT calculations were performed with the Gaussian 16 Rev C.01⁵¹ or ORCA 4.2.1⁵² quantum chemistry programs.

Synthesis of iron(IV)-TAAD complex 1. To a mixture of TAAD·HCl (107 mg, 0.4 mmol), TACN·3HCl (96 mg, 0.4 mmol), anhydrous FeCl_3 (64 mg, 0.4 mmol) and proton sponge (856 mg, 4.0 mmol) was added methanol (10 mL). The reaction mixture was stirred for 1 hour at room temperature under air and then kept for additional 24 hours with a closed cap. The precipitate was centrifuged off and a clear solution

containing complex **1** was concentrated in a vacuum. The residue was dried at 0.1 Torr for 30 min and a mixture of Et₂O (40 mL) and CH₂Cl₂ (40 mL) was added to the crude product. The mixture was left to stay in a refrigerator at 4°C for 4 days. Then the precipitate was separated from the mother liquor and dried at 0.1 Torr for 30 min. The resulting solid material was placed in a centrifuge cup and centrifuged with CH₂Cl₂-Et₂O 5:1 mixture (6 × 12 mL). The residual solid was dissolved in 6 mL of methanol (dark maroon solution) and centrifuged. A clear solution was separated from a small amount of undissolved material and concentrated in a vacuum. This operation was repeated with 4 mL of methanol. The solid material was dried in vacuum at 0.1 Torr to give 102 mg (yield: 48 %) of complex **1** as a black solid. Mp. above 260°C. FT-IR (KBr): 3440 (br), 3277 (s), 3126 (s), 2972 (s), 2932 (s), 2876 (s), 1728 (w), 1629 (s), 1456 (s), 1437 (s), 1373 (s), 1265 (m), 1214 (m), 1175 (m), 1162 (m), 1103 (s), 1070 (w), 1033 (s), 965 (s), 873 (w), 826 (s), 800 (m), 775 (w), 750 (m), 697 (s), 633 (s), 606 (m), 586 (w), 540 (s), 504 (s), 473 (w), 420 (s). UV-vis spectrum: (MeOH, c = 5.9 × 10⁻³ M) peaks λ nm: 345, 496, 577. Mössbauer spectrum, 295K: δ, (mm/s) = 0.2745; |ΔE_Q|, (mm/s) = 3.2089. ESI-HRMS m/z: [M-Cl]⁺ Calcd for [C₁₅H₃₀FeN₇O₃]⁺ 412.1754; Found 412.1753. Anal. Calcd for C₁₅H₃₀ClFeN₇O₃·2CH₃OH·H₂O: C, 38.54; H, 7.61; N, 18.51. Found: C, 38.79; H, 7.26; N, 18.85. *Preparation of crystals for X-ray analysis:* complex **1** (50 mg) was dissolved in 1 mL of methanol and the solution was filtered through a syringe filter. Slow vapor diffusion of diethyl ether into the methanol solution produced black crystals of **1**·CH₃OH suitable for X-Ray diffraction analysis.

Synthesis of complex 3a. To a mixture of quaternary salt **4a** (62 mg, 0.09 mmol), TACN·3HCl (22 mg, 0.09 mmol), anhydrous FeCl₃ (14 mg, 0.09 mmol) and proton sponge (193 mg, 0.9 mmol) was added methanol (2.5 mL). The reaction mixture was stirred for 1 hour at room temperature under air and then kept for additional 24 hours with a closed cap. The precipitate was centrifuged off and clear solution containing complex **3a** was concentrated in a vacuum. The residue was dried at 0.1 Torr for 30 min and a mixture of Et₂O (10 mL) and CH₂Cl₂ (10 mL) was added to the crude product. The mixture was left to stay in a refrigerator at 4°C for 10 days. Then precipitate was separated from mother liquor and dried at 0.1 Torr for 30 min. The residue was placed in a centrifuge cup and centrifuged with CH₂Cl₂-Et₂O 5:1 mixture (3 × 6 mL). The residual solid was dissolved in 1.5 mL of methanol (dark maroon solution) and

centrifuged. Clear solution was separated from small amount of undissolved material and concentrated in vacuum. Solid material was dried in vacuum at 0.1 Torr to give 38 mg (yield 46%) of complex **3a** as a black solid. Mp. above 260°C. FT-IR (KBr): 3436 (br), 2933 (br), 1728 (s), 1667 (s), 1633 (s), 1582 (m), 1455 (s), 1376 (s), 1245 (s), 1199 (w), 1178 (w), 1101 (m), 1035 (s), 1014 (m), 964 (s), 908 (w), 877 (w), 834 (w), 805 (s), 776 (m), 711 (m), 649 (m), 610 (m), 591 (m), 543 (w), 510 (m), 484 (m), 422 (m). UV-vis spectrum: (MeOH, $c = 3.0 \times 10^{-3}$ M) peaks λ nm: 240, 297, 344, 491. Mössbauer spectrum, 295K: δ , (mm/s) = 0.2007; $|\Delta E_Q|$, (mm/s) = 3.0904 ESI-HRMS m/z : $[M-Cl-Br]^{2+}$ Calcd for $[C_{38}H_{61}FeN_7O_6]^{2+}$ 383.7011; Found 383.7009. $[M-Cl-Br-H]^+$ Calcd for $[C_{38}H_{60}FeN_7O_6]^+$ 766.3950; Found 766.3924. Anal. Calcd for $C_{38}H_{61}BrClFeN_7O_6 \cdot 2CH_3OH \cdot 2H_2O$: C, 48.86; H, 7.48; N, 9.97. Found: C, 47.99; H, 7.42; N, 10.53.

Synthesis (2-bromoacetyl)glycylglycylglycine (2b). To a suspension of glycylglycylglycine (55 mg, 0.29 mmol) in water (0.5 mL) and acetone (0.5 mL) was added K_2CO_3 (81 mg, 0.59 mmol). Then reaction mixture was cooled to 0°C and 2-bromoacetyl chloride (300 μ L, 0.36 mmol) was added dropwise. The resulting mixture was stirred at 0°C for 2 hours. Then acetone was removed under reduced pressure and residue was acidified to pH = 2 with 36% wt. aqueous HCl solution (approx. 5 drops). The mixture was left to stay in a refrigerator at 4°C for 8 hours. Then precipitate was separated from mother liquor, washed with acetone (2 \times 500 μ L) and dried in vacuum at 0.1 Torr to give 76 mg (yield: 84%) of **2b** as a white solid. Mp. 215-220°C. 1H NMR (300 MHz, DMSO- d_6 , δ , ppm): 3.74 (m, 6 H), 4.13 (s, 2 H), *NH* and *OH* protons are not observed. FT-IR (KBr): 3276 (s, br), 3087 (s, br), 1718 (s), 1645 (s), 1560 (s), 1422 (s), 1406 (s), 1379 (m), 1337 (w), 1286 (s), 1242 (s, br), 1145 (m), 1089 (w), 1032 (s), 904 (s, br), 791 (m), 700 (s, br), 591 (m), 553 (s), 483 (m). ESI-HRMS m/z : $[M+Na]^+$ Calcd for $[C_8H_{12}BrN_3O_8Na]^+$ 331.9849; Found 331.9853.

Synthesis of quaternary salt 4b. To a suspension of **2b** (60 mg, 0.19 mmol) in water (1 mL) and methanol (1 mL) was added TAAD (45 mg, 0.19 mmol). The reaction mixture was stirred for 120 hours at room temperature. Then KI (32 mg, 0.19 mmol) was added and the reaction mixture was stirred for additional 24 hours at room temperature and afterwards was concentrated under reduced pressure. The residue was dried in a vacuum until constant weight to give 114 mg of mixture **4b** and KI as a yellow

oil, which was used without further purification in the next stage. ^1H NMR (300 MHz, DMSO- d_6 , δ , ppm): 1.25 (s, 9 H), 3.60-3.64 (br, 6 H), 3.76 and 3.84 (2 m, 4 H and 2 H), 4.17 (s, 2 H), *NH* and *OH* protons are not observed. ESI-HRMS m/z : $[\text{M-Br}]^+$ Calcd for $[\text{C}_{17}\text{H}_{30}\text{N}_7\text{O}_8]^+$ 460.2150; Found 460.2141.

Synthesis of complex 3b. To a mixture of **4b** and KI from the previous step (112 mg of mixture containing 80 mg of **4b**, 0.15 mmol), TACN \cdot 3HCl (37 mg, 0.15 mmol), anhydrous FeCl_3 (24 mg, 0.15 mmol) and proton sponge (265 mg, 1.24 mmol) were added 2 mL of methanol and 2 mL of water. The reaction mixture was stirred for 1 hour at room temperature under air and then kept for additional 24 hours with a closed cap. The precipitate was centrifuged off and a clear solution containing complex **3b** was concentrated in a vacuum. The residue was dried at 0.1 Torr for 30 min and a mixture of Et_2O (20 mL) and CH_2Cl_2 (20 mL) was added to the crude product. The mixture was left to stay in a refrigerator at 4°C for 4 days. Then the precipitate was separated from the mother liquor and dried at 0.1 Torr for 30 min. The residue was placed in a centrifuge cup and centrifuged with CH_2Cl_2 (3×10 mL). The residual solid was dissolved in 3 mL of methanol (dark maroon solution) and centrifuged. The clear solution was separated from a small amount of undissolved material and concentrated in a vacuum. The solid material was dried in vacuum at 0.1 Torr to give 64 mg of crude complex **3b**. Black solid. Mp. above 260°C . FT-IR (KBr): 3470 (br), 3272 (br), 2930 (m), 1727 (s), 1663 (s, br), 1568 (s), 1549 (s), 1454 (s), 1376 (s), 1337 (w), 1269 (s), 1238 (s), 1181 (w), 1102 (s), 1032 (s), 965 (s), 872 (m), 822 (m), 806 (s), 774 (s), 743 (m), 706 (s), 650 (m), 633 (m), 609 (m), 585 (m, br), 540 (s), 512 (s), 482 (s), 421 (s). Mössbauer spectrum, 293K: δ , (mm/s) = 0.1983; $|\Delta E_Q|$, (mm/s) = 3.1145. ESI-HRMS m/z : $[\text{M-Cl-Br}]^{2+}$ Calcd for $[\text{C}_{23}\text{H}_{42}\text{FeN}_{10}\text{O}_8]^{2+}$ 321.1263; Found 321.1274. $[\text{M-Cl-Br-H}]^+$ Calcd for $[\text{C}_{23}\text{H}_{41}\text{FeN}_{10}\text{O}_8]^+$ 641.2453; Found 641.2449.

Synthesis of polymer supported complex 3c. To a mixture of polymer PS- CH_2 -TAAD (153 mg, 72% loading of TAAD, ca. 0.1 mmol), TACN \cdot 3HCl (24 mg, 0.1 mmol), anhydrous FeCl_3 (16 mg, 0.1 mmol) and proton sponge (214 mg, 1.0 mmol) were added 2 mL of methanol and 1 mL of THF. The reaction mixture was stirred for 4 hours at room temperature under air and then kept for 17 hours with a closed cap. Thereafter the mixture was stirred for additional 8 hours at room temperature under air. Then the

polymeric material was filtered off using a sorbent-free PrepSep column and washed with 10 mL of THF. The residual solid was dried in vacuum at 0.1 Torr to give 185 mg of polymer **3c** as a black solid. FT-IR (KBr): 3433 (br), 3082 (s), 3061 (m), 3025 (m), 2923 (s), 2854 (s), 1944 (m), 1871 (m), 1803 (m), 1729 (m), 1630 (s), 1601 (s), 1548 (w), 1492 (s), 1451 (s), 1374 (s), 1322 (m), 1268 (m), 1234 (m), 1176 (m), 1156 (m), 1110 (m), 1062 (s), 1028 (s), 986 (s), 973 (s), 944 (s), 906 (m), 870 (w), 832 (m), 795 (s), 755 (s), 698 (s), 650 (m), 615 (m), 537 (s, br), 482 (m), 421 (m). Mössbauer spectrum, 293K: δ , (mm/s) = 0.2040; $|\Delta E_Q|$, (mm/s) = 3.0992. Anal. Found Fe, 3.5; N, 5.70 (29% loading of complex **1**, calculated based on elemental analysis and Mössbauer spectral data).

Aerobic oxidation of *p*-thiocresol catalyzed by complex **1.** *p*-Thiocresol (25 mg, 0.20 mmol, 100 equiv.) and Et₃N (19 mg, 0.19 mmol, 100 equiv.) were added to a 1 mM solution of complex **1** in methanol (2 mL, 0.002 mmol, 1 equiv.). The mixture was stirred in a closed vessel equipped with a magnetic stirrer and an air-filled balloon for 24 hours. The resulting solution was concentrated under reduced pressure. Hexane (2 mL) and water (1 mL) were added to the residue and the mixture was intensively shaken. The organic phase was collected and the aqueous layer was washed with hexane (2 × 2 mL). The combined organic phase was dried over sodium sulfate, concentrated under reduced pressure and dried until constant weight to give 21 mg (84 %) of *p*-tolyl disulfide as a white solid. Mp. 46 °C (Lit.⁵³ 43–46 °C). GC-MS: retention time 10.01 min; m/z = 246 ([M]⁺). ¹H NMR (300 MHz, CDCl₃, δ , ppm): 2.36 (s, 6 H), 7.14 (m, 4 H), 7.43 (m, 4 H). ¹H NMR spectrum is in agreement with literature data.⁵³

Aerobic oxidation of *p*-thiocresol catalyzed by polymer-supported complex **3c.** To a solution of *p*-thiocresol (24 mg, 0.20 mmol) in methanol (1 mL) was added polymer-supported complex **3c** (10 mg, 3 mol% Fe). The mixture was stirred in a closed vessel equipped with a magnetic stirrer and an air-filled balloon for 24 hours. The resulting mixture was concentrated under reduced pressure. Hexane (2 mL) and water (1 mL) were added to the residue and the mixture was intensively shaken. The organic phase was collected and the aqueous layer was washed with hexane (2 × 2 mL). The combined organic phase was dried over sodium sulfate, concentrated under reduced pressure and dried until constant weight to

give 23 mg (98%) of *p*-tolyl disulfide as a white solid. GC-MS and ^1H NMR data are in agreement with the sample prepared by the reaction catalyzed with complex **1** (see previous procedure).

Aerobic oxidation of *n*-heptanethiol catalyzed by complex 1. *n*-Heptanethiol (21 mg, 0.16 mmol, 25 μL , 20 equiv.) and Et_3N (16 mg, 0.16 mmol, 20 equiv.) were added to a 4 mM solution of **1** in methanol (2 mL, 0.008 mmol, 1 equiv.). The mixture was stirred in a closed vessel equipped with a magnetic stirrer and an air-filled balloon for 24 hours. The resulting solution was evaporated with airflow at room temperature. Diethyl ether (1 mL) and water (1 mL) were added to the residue and the mixture was intensively shaken. The organic phase was collected and the aqueous layer was washed with diethyl ether (2×1 mL). The combined organic phase was dried over sodium sulfate. The solvent was evaporated with airflow at room temperature until constant weight to give 15 mg (72 %) of *n*-heptyl disulfide as a yellow oil. GC-MS: retention time 9.38 min; $m/z = 262$ ($[\text{M}]^{+*}$). ^1H NMR (300 MHz, CDCl_3 , δ , ppm): 0.86 – 0.91 (t, $J = 6.8$ Hz, 6H), 1.28 – 1.40 (br m, 16H), 1.67 (m, 4H), 2.66 – 2.71 (t, $J = 7.3$ Hz, 4H). ^1H NMR spectrum is in agreement with literature data.⁵⁴

Aerobic oxidation of glutathione catalyzed by complex 1. Glutathione GSH (27 mg, 0.087 mmol, 20 equiv.) and NaHCO_3 (21 mg, 0.26 mmol, 60 equiv.) were added to a 1 mM solution of **1** in water (4.35 mL, 4.35 μmol , 1 equiv.). The reaction mixture was stirred in a closed vessel equipped with a magnetic stirrer and an air-filled balloon for 24 hours. The resulting solution was concentrated under reduced pressure and MeOH was added to the residue. The resulting precipitate was separated from the solution and washed with MeOH until the solution became colorless. The residual solid was dried under reduced pressure to give 25 mg (83%) of GSSG sodium salt as a white solid. ^1H NMR (300 MHz, D_2O , δ , ppm): 1.95 (m, 4H), 2.25–2.52 (m, 4H), 2.87 (dd, $J = 14.3, 9.7$ Hz, 2H), 3.21 (dd, $J = 14.3, 4.5$ Hz, 2H), 3.45 (t, $J = 6.3$ Hz, 2H), 3.65 (d, $J = 20.9$ Hz, 2H), 3.72 (d, $J = 20.9$ Hz, 2H), 4.67 (m, 2H). ^1H NMR spectrum of glutathione disulfide is in agreement with literature data.⁵⁵

Acknowledgments

This work was supported by the Russian Foundation for Basic Research (grant 20-03-00510_a). X-ray diffraction data were collected with financial support from the Ministry of Science and Higher Education of the Russian Federation using the equipment of the Center for molecular composition studies of INEOS RAS. Mossbauer spectroscopy studies were supported by the Russian Ministry of Science and Higher Education within the State assignment of the FSRC “Crystallography and Photonics” of RAS.

References

1. M. Costas, M. P. Mehn, M. P. Jensen and L. Que, *Chem. Rev.*, 2004, **104**, 939-986.
2. E. I. Solomon, S. Goudarzi and K. D. Sutherlin, *Biochemistry*, 2016, **55**, 6363-6374.
3. E. N. Cook, D. A. Dickie and C. W. Machan, *J. Am. Chem. Soc.*, 2021, **143**, 16411-16418.
4. D. P. Galonić, E. W. Barr, C. T. Walsh, J. M. Bollinger and C. Krebs, *Nat. Chem. Biol.*, 2007, **3**, 113-116.
5. W. Zhu, S. Jang, J. Xiong, R. Ezhov, X.-X. Li, T. Kim, M. S. Seo, Y.-M. Lee, Y. Pushkar, R. Sarangi, Y. Guo and W. Nam, *J. Am. Chem. Soc.*, 2021, **143**, 15556-15561.
6. M. C. Simons, S. D. Prinslow, M. Babucci, A. S. Hoffman, J. Hong, J. G. Vitillo, S. R. Bare, B. C. Gates, C. C. Lu, L. Gagliardi and A. Bhan, *J. Am. Chem. Soc.*, 2021, **143**, 12165-12174.
7. J. L. Lee, D. L. Ross, S. K. Barman, J. W. Ziller and A. S. Borovik, *Inorg. Chem.*, 2021, **60**, 13759-13783.
8. N. P. Dunham and F. H. Arnold, *ACS Catal.*, 2020, **10**, 12239-12255.
9. A. J. Jasniewski and L. Que, *Chem. Rev.*, 2018, **118**, 2554-2592.
10. J. Hohenberger, K. Ray and K. Meyer, *Nat. Commun.*, 2012, **3**, 720.
11. M. Srnec, S. R. Iyer, L. M. K. Dassama, K. Park, S. D. Wong, K. D. Sutherlin, Y. Yoda, Y. Kobayashi, M. Kurokuzu, M. Saito, M. Seto, C. Krebs, J. M. Bollinger and E. I. Solomon, *J. Am. Chem. Soc.*, 2020, **142**, 18886-18896.
12. V. F. Oswald, J. L. Lee, S. Biswas, A. C. Weitz, K. Mittra, R. Fan, J. Li, J. Zhao, M. Y. Hu, E. E. Alp, E. L. Bominaar, Y. Guo, M. T. Green, M. P. Hendrich and A. S. Borovik, *J. Am. Chem. Soc.*, 2020, **142**, 11804-11817.
13. J. England, J. O. Bigelow, K. M. Van Heuvelen, E. R. Farquhar, M. Martinho, K. K. Meier, J. R. Frisch, E. Münck and L. Que, *Chem. Sci.*, 2014, **5**, 1204-1215.
14. A. R. McDonald and L. Que Jr, *Coord. Chem. Rev.*, 2013, **257**, 414-428.
15. A. Chanda, X. Shan, M. Chakrabarti, W. C. Ellis, D. L. Popescu, F. Tiago de Oliveira, D. Wang, L. Que, T. J. Collins, E. Münck and E. L. Bominaar, *Inorg. Chem.*, 2008, **47**, 3669-3678.
16. F. T. De Oliveira, A. Chanda, D. Banerjee, X. Shan, S. Mondal, L. Que, E. L. Bominaar, E. Münck and T. J. Collins, *Science*, 2007, **315**, 835-838.
17. J. Bautz, M. R. Bukowski, M. Kerscher, A. Stubna, P. Comba, A. Lienke, E. Münck and L. Que Jr., *Angew. Chem. Int. Ed.*, 2006, **45**, 5681-5684.
18. M. R. Bukowski, K. D. Koehntop, A. Stubna, E. L. Bominaar, J. A. Halfen, E. Münck, W. Nam and L. Que, *Science*, 2005, **310**, 1000-1002.

19. J.-U. Rohde, J.-H. In, M. H. Lim, W. W. Brennessel, M. R. Bukowski, A. Stubna, E. Münck, W. Nam and L. Que, *Science*, 2003, **299**, 1037-1039.
20. S. Tomyň, S. I. Shylin, D. Bykov, V. Ksenofontov, E. Gumienna-Kontecka, V. Bon and I. O. Fritsky, *Nat. Commun.*, 2017, **8**, 1-9.
21. S. I. Shylin, M. V. Pavliuk, L. D'Amario, F. Mamedov, J. Sá, G. Berggren and I. O. Fritsky, *Chem. Commun.*, 2019, **55**, 3335-3338.
22. I. S. Golovanov, R. S. Malykhin, V. K. Lesnikov, Y. V. Nelyubina, V. V. Novikov, K. V. Frolov, A. I. Stadnichenko, E. V. Tretyakov, S. L. Ioffe and A. Y. Sukhorukov, *Inorg. Chem.*, 2021, **60**, 5523-5537.
23. A. N. Semakin, A. Y. Sukhorukov, A. V. Lesiv, S. L. Ioffe, K. A. Lyssenko, Y. V. Nelyubina and V. A. Tartakovsky, *Org. Lett.*, 2009, **11**, 4072-4075.
24. I. S. Golovanov, A. Y. Sukhorukov, Y. V. Nelyubina, Y. A. Khomutova, S. L. Ioffe and V. A. Tartakovsky, *J. Org. Chem.*, 2015, **80**, 6728-6736.
25. D. Premužić, M. Hołyńska, A. Ozarowski, C. Pietzonka, A. Roseborough and S. A. Stoian, *Inorg. Chem.*, 2020, **59**, 10768-10784.
26. E. Samoľová, D. Premužić, S. Pociennik and M. Hołyńska, *J. Mol. Struct.*, 2019, **1176**, 366-375.
27. I. S. Golovanov, G. S. Mazeina, Y. V. Nelyubina, R. A. Novikov, A. S. Mazur, S. N. Britvin, V. A. Tartakovsky, S. L. Ioffe and A. Y. Sukhorukov, *J. Org. Chem.*, 2018, **83**, 9756-9773.
28. R. H. de Vries, J. H. Viel, O. P. Kuipers and G. Roelfes, *Angew. Chem. Int. Ed.*, 2021, **60**, 3946-3950.
29. I. A. Gass, C. J. Gartshore, D. W. Lupton, B. Moubaraki, A. Nafady, A. M. Bond, J. F. Boas, J. D. Cashion, C. Milsmann, K. Wieghardt and K. S. Murray, *Inorg. Chem.*, 2011, **50**, 3052-3064.
30. T.-A. D. Nguyen, A. M. Wright, J. S. Page, G. Wu and T. W. Hayton, *Inorg. Chem.*, 2014, **53**, 11377-11387.
31. C. N. Verani, E. Rentschler, T. Weyhermüller, E. Bill and P. Chaudhuri, *J. Chem. Soc., Dalton Trans.*, 2000, 4263-4271.
32. J. J. Scepaniak, A. M. Wright, R. A. Lewis, G. Wu and T. W. Hayton, *J. Am. Chem. Soc.*, 2012, **134**, 19350-19353.
33. G. Bulaj, *Biotechnol. Adv.*, 2005, **23**, 87-92.
34. G. Wu, Y.-Z. Fang, S. Yang, J. R. Lupton and N. D. Turner, *J. Nutr.*, 2004, **134**, 489-492.
35. Q. Wang, J. Guan, J. Wan and Z. Li, *RSC Advances*, 2020, **10**, 24397-24409.
36. E. Anon, *Agrichem Age*, 1989, **33**, 20.
37. Y. Zhang, D. Yang, Y. Li, X. Zhao, B. Wang and J. Qu, *Catal. Sci. Technol.*, 2019, **9**, 6492-6502.
38. A. Corma, T. Ródenas and M. J. Sabater, *Chem. Sci.*, 2012, **3**, 398-404.
39. H. Huang, J. Ash and J. Y. Kang, *Org. Biomol. Chem.*, 2018, **16**, 4236-4242.
40. A. N. Semakin, I. S. Golovanov, A. Y. Sukhorukov, S. L. Ioffe and V. A. Tartakovsky, *Russ. Chem. Bull.*, 2016, **65**, 2270-2277.
41. X. Zhang, Z. Zuo, J. Tang, K. Wang, C. Wang, W. Chen, C. Li, W. Xu, X. Xiong, K. Yuntai, J. Huang, X. Lan and H.-B. Zhou, *Bioorg. Med. Chem. Lett.*, 2013, **23**, 3793-3797.
42. L. M. De León-Rodríguez and Z. Kovacs, *Bioconjugate Chem.*, 2008, **19**, 391-402.
43. V. V. Ozerova, I. S. Zhidkov, A. Boldyreva, N. N. Dremova, N. A. Emelianov, G. V. Shilov, L. A. Frolova, E. Z. Kurmaev, A. Y. Sukhorukov, S. M. Aldoshin and P. A. Troshin, *Energies*, 2021, **14**, 669.
44. A. S. Komendantova, A. M. Scherbakov, A. V. Komkov, V. V. Chertkova, A. O. Gudovanniy, E. I. Chernoburova, D. V. Sorokin, Y. U. Dzichenka, V. Z. Shirinian, Y. A. Volkova and I. V. Zavarzin, *Bioorg. Chem.*, 2019, **91**, 103142.
45. P. Jiao, P. Jin, C. Li, L. Cui, L. Dong, B. Pan, W. Song, L. Ma, J. Dong, L. Song, X. Jin, F. Li, M. Wan, Z. Lv and Q. Geng, *Bioorg. Med. Chem. Lett.*, 2016, **26**, 4679-4683.
46. D. Evans, *J. Chem. Soc.*, 1959, 2003-2005.
47. C. Piguet, *J. Chem. Educ.*, 1997, **74**, 815.
48. G. A. Bain and J. F. Berry, *J. Chem. Educ.*, 2008, **85**, 532.
49. P. G. Naumov, I. S. Lyubutin, K. V. Frolov and E. I. Demikhov, *Instrum. Exp. Tech.*, 2010, **53**, 770-776.
50. A. Coelho, TOPAS 4.2, Bruker AXS GmbH, Karlsruhe, Germany, 2009.

51. M. J. Frisch, G. W. Trucks, H. B. Schlegel, G. E. Scuseria, M. A. Robb, J. R. Cheeseman, G. Scalmani, V. Barone, G. A. Petersson, H. Nakatsuji, X. Li, M. Caricato, A. V. Marenich, J. Bloino, B. G. Janesko, R. Gomperts, B. Mennucci, H. P. Hratchian, J. V. Ortiz, A. F. Izmaylov, J. L. Sonnenberg, Williams, F. Ding, F. Lipparini, F. Egidi, J. Goings, B. Peng, A. Petrone, T. Henderson, D. Ranasinghe, V. G. Zakrzewski, J. Gao, N. Rega, G. Zheng, W. Liang, M. Hada, M. Ehara, K. Toyota, R. Fukuda, J. Hasegawa, M. Ishida, T. Nakajima, Y. Honda, O. Kitao, H. Nakai, T. Vreven, K. Throssell, J. A. Montgomery Jr., J. E. Peralta, F. Ogliaro, M. J. Bearpark, J. J. Heyd, E. N. Brothers, K. N. Kudin, V. N. Staroverov, T. A. Keith, R. Kobayashi, J. Normand, K. Raghavachari, A. P. Rendell, J. C. Burant, S. S. Iyengar, J. Tomasi, M. Cossi, J. M. Millam, M. Klene, C. Adamo, R. Cammi, J. W. Ochterski, R. L. Martin, K. Morokuma, O. Farkas, J. B. Foresman and D. J. Fox, *Gaussian 16, Revision C.01*, Gaussian, Inc., Wallingford CT, 2016.
52. F. Neese, *WIREs Comput. Mol. Sci*, 2018, **8**, e1327.
53. N. Iranpoor, H. Firouzabadi and A. Jamalian, *Synlett*, 2005, **2005**, 1447-1449.
54. I. Steinfatt, G. G. Hoffmann, L. Brouwer, F. Menzel and W. Brockner, *Phosphorus Sulfur Silicon Relat. Elem.*, 1998, **134**, 31-55.
55. S.-Y. Cui, H. Jin, S.-J. Kim, A. P. Kumar and Y.-I. Lee, *J. Biochem.*, 2008, **143**, 685-693.